Superconductor Science and Technology

PAPER

Superconducting electrode capacitor based on double-sided YBCO thin film for wireless power transfer applications

To cite this article: Yingda He *et al* 2019 *Supercond. Sci. Technol.* **32** 015010

IOP Publishing Superconductor Science and Technology
Supercond. Sci. Technol. 32 (2019) 039502 (2pp) https://doi.org/10.1088/1361-6668/aafef4

Corrigendum: Superconducting electrode capacitor based on double-sided YBCO thin film for wireless power transfer applications (2019 *Supercond. Sci. Technol.* 32 015010)

Yingda He[1], Yu Wang[1,2,3], Yanwen Hu[1], Weirong Chen[1] and Zhongming Yan[1]

[1] School of Electrical Engineering, Southwest Jiaotong University, Chengdu 611756, People's Republic of China
[2] Key Laboratory of Magnetic Suspension Technology and Maglev Vehicle, Ministry of Education, Southwest Jiaotong University, Chengdu 611756, People's Republic of China

E-mail: wangyu@swjtu.edu.cn

Received 8 January 2019
Accepted for publication 16 January 2019
Published 31 January 2019

(Some figures may appear in colour only in the online journal)

The correct figure 7 is shown in this corrigendum. The statement 'These gaps attain the maximum…' in section 4.1.2 should be 'The Q-factor gap between the HTS capacitor and the CBB bank attains the maximum…'.

Since all the numerical evaluations about the HTS capacitor in section 4 were based on the correct figure 7, the results and conclusions in the original article remain the same.

[3] Author to whom any correspondence should be addressed.

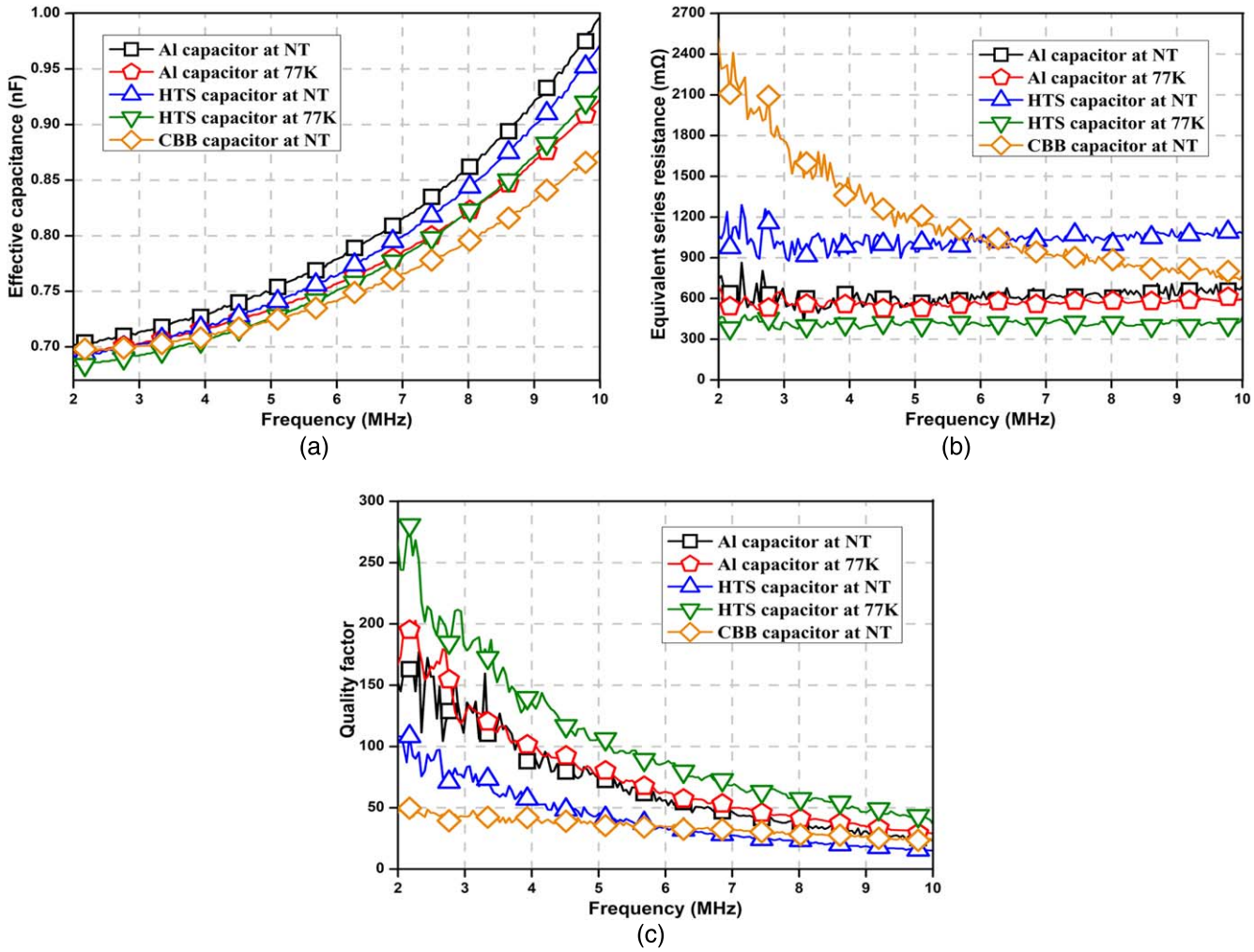

Figure 7. Measured characteristics of the HTS capacitor and contrasting capacitors. (a) Effective capacitance. (b) ESR. (c) Q-factor.

ORCID iDs

Yingda He https://orcid.org/0000-0002-0963-4160
Yu Wang https://orcid.org/0000-0002-5391-8603
Yanwen Hu https://orcid.org/0000-0003-1557-6064
Zhongming Yan https://orcid.org/0000-0002-9879-2792

IOP Publishing Superconductor Science and Technology
Supercond. Sci. Technol. 32 (2019) 015010 (10pp) https://doi.org/10.1088/1361-6668/aaebd8

Superconducting electrode capacitor based on double-sided YBCO thin film for wireless power transfer applications

Yingda He[1], Yu Wang[1,2,3], Yanwen Hu[1], Weirong Chen[1] and Zhongming Yan[1]

[1] School of Electrical Engineering, Southwest Jiaotong University, Chengdu 611756, People's Republic of China
[2] Key Laboratory of Magnetic Suspension Technology and Maglev Vehicle, Ministry of Education, Southwest Jiaotong University, Chengdu 611756, People's Republic of China

E-mail: wangyu@swjtu.edu.cn

Received 6 June 2018, revised 17 October 2018
Accepted for publication 26 October 2018
Published 29 November 2018

Abstract

A high-temperature superconducting (HTS) electrode capacitor (HTS capacitor) has been reported for the first time in the form of a superconductor–insulator–superconductor structure. Double-sided HTS thin film might be inherently suitable for the raw material choice of an HTS capacitor. In terms of electrode material, HTS thin film has a much lower surface resistance than normal conductors, and, as a dielectric medium, its substrate generally has a larger dielectric constant but a smaller loss tangent than the dielectric layers of some conventional capacitors. Thus, it is possible to fabricate a high-quality capacitor based on double-sided HTS thin film. This type of HTS capacitor could play a role in wireless power transfer (WPT) technology, since the WPT efficiency depends on the quality factors of both the coil and capacitor. Numerous studies have been performed to optimize the WPT system with HTS coil. In contrast, we develop an HTS capacitor based on double-sided YBCO film for WPT applications and investigate its effect on the WPT system. It is found that the HTS capacitor can provide a high quality factor, enhance WPT efficiency, and work normally with an HTS coil at 77 K, avoiding the dilemma between an HTS coil and a normal capacitor.

Keywords: superconducting electrode capacitor, double-sided YBCO thin film, wireless power transfer

(Some figures may appear in colour only in the online journal)

1. Introduction

With the development of high-temperature superconducting (HTS) technology, HTS materials have been utilized in multiple kinds of electric equipment as well as electronic devices due to their advantages of low loss, high critical current density, and other application properties [1]. Those devices (transformers, generators, filters, etc) can achieve a better performance by fabricating their conductive components using superconductors. Meanwhile, some research efforts have been made to apply HTS materials to capacitors commonly used in electric and electronic fields. Since the basic structure of a capacitor is in the form of conductor–insulator–conductor, HTS materials can be used to fabricate the electrode plates of a capacitor, referred to as a HTS electrode capacitor ('HTS capacitor' for short). In general, the loss of a capacitor at high frequency is derived mainly from the dielectric layer as well as the electrode plates [2, 3]. Note that the surface resistance of HTS materials is much lower than that of normal conductors over a frequency range up to GHz level [4, 5]. The HTS electrode plates can enable the capacitor to achieve a higher quality factor (Q-factor).

In 1991, Jones *et al* [6] proposed a prototype of a HTS capacitor based on a superconductor–insulator–superconductor

[3] Author to whom any correspondence should be addressed.

multilayer structure ($YBa_2Cu_3O_{7-x}$-$YBaCuO_5$-$YBa_2Cu_3O_{7-x}$) which was found to be capacitive at 77 K, and described it as a low loss high-frequency capacitor. However, no experimental results were revealed to verify its benefit or applications. Some subsequent studies were performed on an HTS capacitor formed by $YBa_2Cu_3O_{7-x}$ (YBCO) thin film deposited on ferroelectric substrate. It was found that the superconductor–ferroelectric–superconductor (SFS) based capacitor had a capacitance dependence on the DC bias voltage [7, 8]. In addition, there were other proposals for designing a capacitor with single-sided YBCO film [9–11]. Specifically, superconductor/ferroelectric film-based planar capacitors were designed in [9, 10] for microwave applications, while a capacitor based on a superconductor–ferroelectric–conductor structure was reported in [11] with the capacitance characteristic observed in a radiation environment.

A major issue encountered in HTS applications, especially large-scale industrial ones, is the leakage heat through current leads [12, 13]. The HTS capacitor has the potential to serve as a fundamental element to form an all-superconducting system or circuit with other HTS devices. For those HTS devices in need of a capacitor, an HTS capacitor can work with them in one adiabatic chamber without current leads linking to the external environment, thus reducing the leakage heat as well as enhancing the cooling efficiency compared to a conventional capacitor. Namely, it can avoid the additional fabrication cost and operation cost caused by leads between a cooling environment and an external one.

In recent years, wireless power transfer (WPT) technology via magnetic resonance coupling [14] has become a research hotspot due to its advantage of providing an efficient contactless way for power delivery near field. Numerous studies on the application of superconducting materials in a WPT field have appeared, since the low loss property of superconductors is attractive for a WPT system in order to improve the efficiency [15–18]. While most of them focused on optimizing the WPT system with an HTS coil, Sedwick [19] proposed the potential application of an HTS capacitor to WPT technology with relevant theoretical analysis, as well as the concept of an all-superconducting oscillator (or resonator) which is composed of a superconducting coil and a 'superconducting capacitor'. For a WPT system, the Q-factor of the resonator has a significant influence on the transfer efficiency [20, 21], depending on the Q-factors of both the coil and capacitor. Thus, an HTS capacitor with a high Q-factor can enhance the WPT efficiency as well.

In this paper, we propose an HTS capacitor based on double-sided YBCO thin film on a lanthanum aluminate ($LaAlO_3$) structure for WPT applications. In contrast to previous studies [7, 8] performed on double-sided YBCO film-based HTS capacitors, this work is the first attempt to apply this type of HTS capacitor to a WPT system. Besides capacitance, other important characteristics of a capacitor for WPT applications, including equivalent series resistance (ESR) and Q-factor, are also measured. The effects of the HTS capacitor on a WPT system are confirmed by comparative experiments. As opposed to the single-sided YBCO film-based capacitors in [9–11], the proposed HTS capacitor aims to serve the WPT applications. Note that a WPT system demands a resonator with low resonant frequency (generally below the microwave range) and a high Q-factor [14]. The double-sided YBCO film-based capacitor can offer a larger capacitance than microwave-used planar capacitors [9, 10] to form a lower resonant frequency with HTS coil, as well as a higher Q-factor than an HTS/metal hybrid-electrode capacitor [11] to reduce the power loss.

In contrast to the theoretical paper [19] that proposed the application of an HTS capacitor to WPT technology, we first perform the experimental investigation on a double-sided YBCO film-based HTS capacitor and a relevant system for WPT applications. In addition, all-superconducting resonators reported so far are almost fabricated from a single patterned HTS film and generally used for microwave applications [22–24], while this work attempts to fabricate and research a novel kind of all-superconducting resonator for WPT applications which consists of an HTS film-based capacitor and HTS tape-based coil.

The following section will describe the structure and properties of the proposed HTS capacitor. The WPT system with the HTS capacitor is presented in section 3, with its principle analyzed theoretically. Furthermore, section 4 shows the details and test results of comparative experiments which are conducted to investigate the characteristics of the HTS capacitor and its effect on the WPT system. A conclusion is drawn at the end of this paper.

2. Superconducting electrode capacitor

2.1. Structure description

The fabrication technique of HTS thin film has developed enough to meet the requirements of superconducting microwave devices up to now [4]. The double-sided HTS thin film deposited on a dielectric substrate can serve as a superconductor–insulator–superconductor structure with a large area as well as high uniformity. In addition to the small surface resistance, it has a substrate which provides a larger dielectric constant but a lower loss tangent than the dielectric layers of some conventional capacitors. These features make it inherently suitable for the raw material choice of an HTS capacitor to achieve a high Q-factor.

As shown in figure 1, the proposed HTS capacitor is based on doubled-sided YBCO thin film whose substrate is $LaAlO_3$ with a low loss tangent. The surface gold (Au) coatings are used to protect the YBCO layers from deterioration in damp conditions and to contribute to the welding of the current leads. Each side of the thin film is etched off at the edge against the substrate for the sake of capacitor insulation.

2.2. Prototype fabrication

The main component of the HTS capacitor prototype is a 2 inch diameter doubled-sided YBCO thin film, and its specifications are listed in table 1. The YBCO film was epitaxially

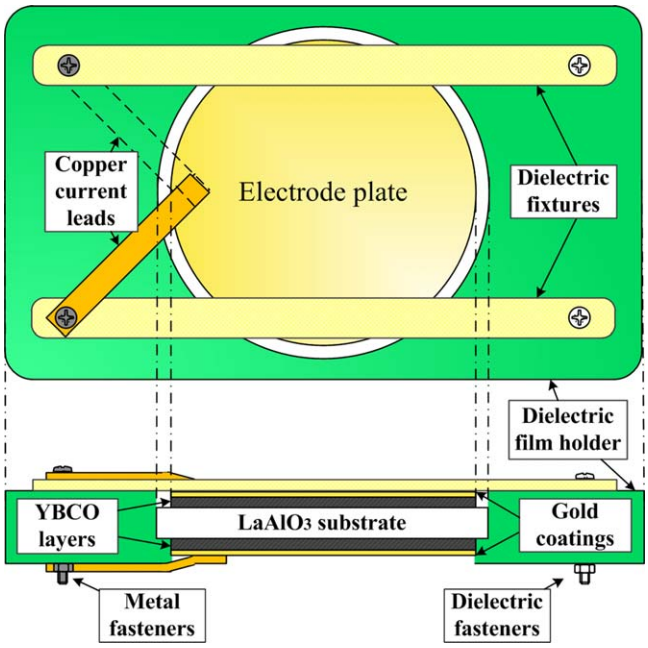

Figure 1. Structure of the proposed HTS capacitor.

Table 1. Specifications of the HTS capacitor.

Parameter	Value	Unit
Radius of the thin film each side	22.5	mm
Thickness of the YBCO layer each side	0.5	μm
Thickness of the Au coating each side	0.1	μm
Radius of the $LaAlO_3$ substrate	25.4	mm
Thickness of the $LaAlO_3$ substrate	0.5	mm
Typical loss tangent of the $LaAlO_3$ substrate	3×10^{-5}	
Typical relative permittivity of the $LaAlO_3$ substrate	23.5	
Width of the current lead	5.5	mm
Length of the current lead	42.5	mm
Thickness of the current lead	0.5	mm

grown on the $LaAlO_3$ substrate by DC sputtering and then surface-coated by a Au protective layer on both sides to prepare for soldering. The superconducting transition temperature of the film is approximately 90 K, and the thickness deviation is less than 3%. In addition, the microwave surface resistance (77 K, 10 GHz) is lower than 0.2 mΩ, and critical current density (77 K, self-field) is larger than 2.8 MA cm^{-2}.

Each side of the edge of the thin film layer (including 0.5 μm-thick YBCO and 0.1 μm-thick Au) was kept 0.29 cm away from the $LaAlO_3$ substrate edge by using an ion beam etching technique in order to increase the creepage distance between both sides of the YBCO film, which serves as HTS electrode plates. After etching, the film was mounted in the circular groove of a dielectric holder and fixed with epoxy resin fixtures as well as dielectric fasteners. During the final step, two copper leads were welded onto the edge of the YBCO film on both sides using an indium solder and then

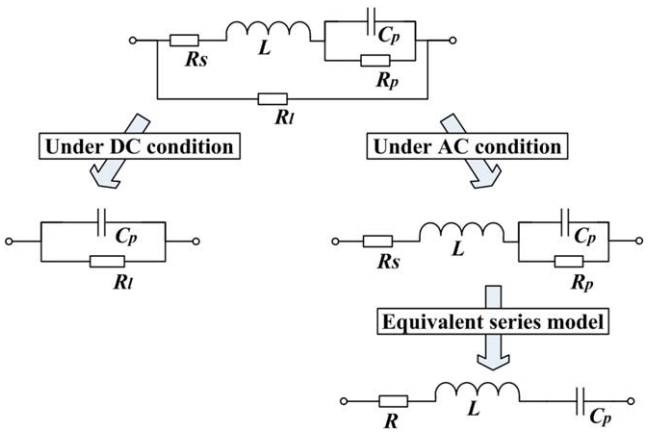

Figure 2. Simplified analysis model of the HTS capacitor.

fixed on the holder by metal fasteners which also act as the lead terminals.

2.3. Analysis model

The proposed HTS capacitor can be regarded as a typical circular parallel-plate capacitor. By applying a lumped circuit element model [2, 3], the analysis model is built and simplified as presented in figure 2. The term C_p represents the capacitance based on the dielectric layer polarization, and L represents the parasitic inductance caused by the electrode plates and current leads. The terms R_s and R_p denote the respective equivalent resistances of the conductive components and dielectric layer. The leakage resistance R_l is related to the DC voltage maintaining the performance of the capacitor [25].

Under DC conditions, the major loss of the capacitor is caused by R_l, and thus the initial model can be analyzed with R_s and R_p neglected. In contrast, the capacitor loss is derived mainly from R_s and R_p under AC conditions. For the sake of a characteristic study, a simplified equivalent series model is deduced from the model under AC conditions. The relevant derivation process is expressed in the form of capacitor impedance at frequency f as follows:

$$\begin{aligned} Z &= R_s + jwL + \frac{1}{jwC_p + R_p^{-1}} \\ &= R_s + \frac{R_p}{1 + w^2C_p^2R_p^2} \\ &\quad + j\left\{wL - \frac{1}{wC_p[1 + 1/(w^2C_p^2R_p^2)]}\right\} \\ &\approx R + j\left(wL - \frac{1}{wC_p}\right) for\ w^2C_p^2R_p^2 \gg 1 \end{aligned} \quad (1)$$

with

$$w = 2\pi f,\ R = R_s + \frac{R_p}{1 + w^2C_p^2R_p^2}$$

where R is the ESR, and w is the angular frequency.

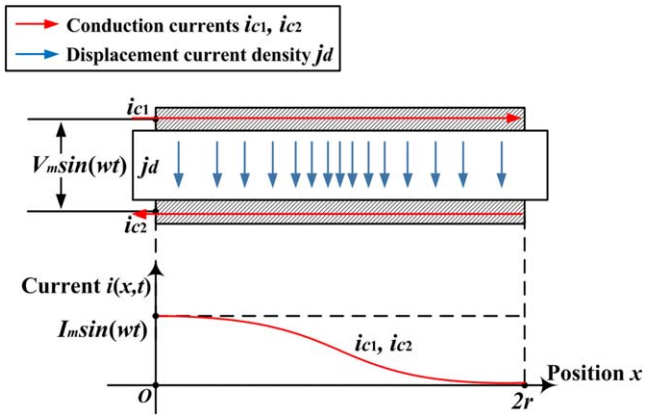

Figure 3. Currents distribution of the HTS capacitor.

Since the relative permittivity ε_r of the dielectric layer is related to f as well as temperature T, C_p can be obtained as:

$$C_p = \frac{\varepsilon_r(w,\ T)\varepsilon_0 \pi r^2}{d} \tag{2}$$

where d represents the thickness of the dielectric layer, r represents the overlap radius of the electrode plates, and ε_0 is the permittivity of vacuum. According to (1), the actual capacitance (or effective capacitance) C of the capacitor in consideration of L can be deduced as:

$$\begin{aligned} Z &= R - jw\frac{1}{C} = R + j\left(wL - \frac{1}{wC_p}\right) \\ \Rightarrow C &= \frac{C_p}{1 - w^2 L C_p}. \end{aligned} \tag{3}$$

In general, it is necessary for C not to change much for the sake of the steady capacitive characteristic versus frequency, thus L should be reduced as little as possible.

The self-resonant frequency f_R of the HTS capacitor can be derived from (3) as follows:

$$C = 0 \Rightarrow f_R = \frac{1}{2\pi\sqrt{LC_p}}. \tag{4}$$

Obviously, the operating frequency of the capacitor is limited to f_R, namely $f < f_R$. Also, the key method to raise the upper limit of the operating frequency is to decrease L. For this, the currents of the HTS capacitor are designed to flow through the electrode plates and leads in an antiparallel direction, as shown in figure 3, achieving negative mutual inductances and thus lowering L.

The total parasitic inductance L of the capacitor is derived from the electrode plates and leads, which is presented as:

$$L = L_{ep} + L_{cl} \tag{5}$$

with

$$L_{ep} = 2(L'_{ep} - M_{ep}),\ L_{cl} = 2(L'_{cl} - M_{cl}) \tag{6}$$

where L_{ep} and L_{cl} represent the respective parasitic inductances of the electrode plate and current lead. The term L_{ep} is a combination of the self-inductance L'_{ep} and mutual inductance M_{ep} of the electrode plate. Similarly, L_{cl} is related to the self-inductance L'_{cl} and mutual inductance M_{cl} of the lead.

2.4. Quality factor

The Q-factor is an important index to evaluate the loss property of a capacitor. As mentioned above, the major loss of an HTS capacitor at high frequency is produced by the electrode plates and substrate, thus the Q-factor can be expressed as:

$$Q = \frac{1}{RwC} = \frac{1}{(R_{ep} + R_{cl})wC + DF_{ds}} \tag{7}$$

where R_{ep} and R_{cl} are the respective ESRs of the electrode plates and current leads, and DF_{ds} is the dissipation factor of the dielectric substrate. Under the condition of fixed w and C, Q has a higher value by reducing R and DF_{ds}. In contrast to normal capacitors, the HTS capacitor can attain a better Q-factor due to the lower surface resistance of the HTS electrode plates as well as the smaller loss tangent of the substrate.

According to the model of the parallel-plate capacitor in [2], the current-space characteristic of the HTS capacitor is shown in figure 3. The conduction currents i_{c1} and i_{c2} flow through the electrode plates in antiparallel directions. The boundary conditions of i_{c1} and i_{c2} are described as:

$$\begin{aligned} &i_{c1}(x,\ t)|_{x=0} = i_{c2}(x,\ t)|_{x=0} = I_m \sin(wt) = \frac{V_m \sin(wt)}{Z}, \\ &i_{c1}(x,\ t)|_{x=2r} = i_{c2}(x,\ t)|_{x=2r} = 0, \\ &\frac{\partial i_{c1}(x,\ t)}{\partial x} = \frac{\partial i_{c2}(x,\ t)}{\partial x} = -2\sqrt{2rx - x^2}\, j_d(t) \end{aligned} \tag{8}$$

where I_m and V_m are the respective amplitude values of the conduction current and voltage, and j_d is the density of the displacement current through the dielectric layer vertically. Considering $\pi r^2 j_d\ (t) = I_m \sin(wt)$, i_{c1} and i_{c2} versus $(x,\ t)$ can be deduced as follows:

$$i_{c1}(x,\ t) = i_{c2}(x,\ t) = D(x) I_m \sin(wt) \tag{9}$$

with

$$D(x) = \frac{\frac{1}{2}\pi r^2 - (r - x)\sqrt{2rx - x^2} + r^2 \text{arc sin}\,\frac{r-x}{r}}{\pi r^2} \tag{10}$$

where D(x) reflects the nonlinear distribution of conductive currents across the electrode plates. By introducing the AC loss of the HTS material, R_{ep} can be defined as:

$$R_{ep} = \frac{2\int_0^{2r} 2\sqrt{2rx - x^2}\, p_{AC}(x)dx}{(I_m/\sqrt{2})^2} \tag{11}$$

where p_{AC} represents the surface power density of the AC loss. When the HTS electrode plates move into the normal state, R_{ep} would become much larger, thus dramatically reducing the Q-factor.

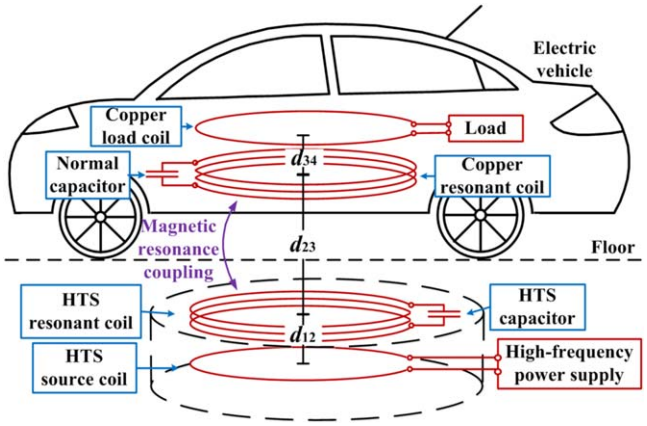

Figure 4. Schematic of the WPT system with the HTS capacitor.

Considering that current leads are two conductive tapes with a rectangular section, R_{cl} can be obtained as follows:

$$R_{cl} = 2\rho_{cl}\frac{l_{cl}}{d_{cle}b_{cl}} \tag{12}$$

where l_{cl}, b_{cl}, ρ_{cl}, and d_{cle} denote the length, width, electric resistivity, and effective thickness of the leads, respectively.

3. WPT system with the HTS capacitor

3.1. System configuration

Since superconducting WPT technology is considered to be a potential candidate for charging electric vehicles [17, 18], the relevant conceptual design of a WPT system with an HTS capacitor is illustrated in figure 4. It is composed of a high-frequency power supply, an HTS source coil, an all-superconducting transmitter, a normal receiver, a copper load coil, and a load. The receiver consists of a copper resonant coil and normal capacitor, while the transmitter is based on an HTS resonant coil and HTS capacitor. The resonators are both designed to operate at the same resonant frequency for the sake of optimal magnetic resonance coupling.

All coils are aligned coaxially, and the distance between the source coil and transmitting coil is the same as that between the load coil and receiving coil, namely $d_{12} = d_{34}$. To avoid the negative impact of metallic obstacles [26, 27], the parts of the adibatic container wall, floor, and vehicle chassis blocking the WPT path should be manufactured with non-metallic materials. The HTS capacitor can work at 77 K, and thus operate with HTS resonant coil in the same environment to avoid heat leakage through the current leads, sustaining the high efficiency of the cooling system.

3.2. Equivalent circuit

The equivalent circuit of the WPT system with the HTS capacitor is shown in figure 5. The term Z_{Load} denotes the load impedance, while V_S and Z_S represent the voltage and internal impedance of the high-frequency power supply, respectively. A two-port network is extracted from the

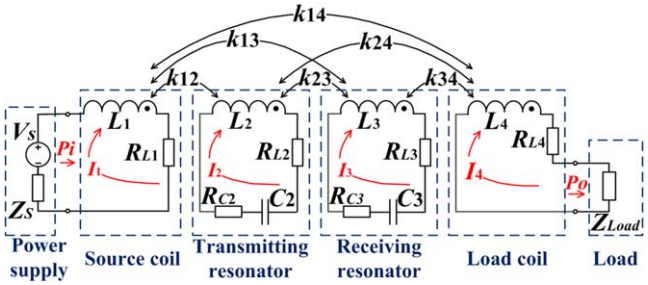

Figure 5. Equivalent circuit of the WPT system.

equivalent circuit, with input and output powers denoted by P_i and P_o, respectively. The terms L_i and R_{Li} ($i = 1, 2, 3, 4$) denote the respective inductances and ESRs of the coils, while C_i and R_{Ci} ($i = 2, 3$) represent the respective effective capacitances and ESRs of the capacitors. In addition, k_{ij} ($i \neq j$ and $i, j = 1, 2, 3, 4$) are the coupling coefficients among these coils.

3.3. Theoretical analysis

By applying Kirchhoff's circuit law, the operating principle of the WPT system at frequency f can be expressed as:

$$\begin{bmatrix}\dot{I}_1 & \dot{I}_2 & \dot{I}_3 & \dot{I}_4\end{bmatrix}\cdot Z = \begin{bmatrix}\dot{V}_S & 0 & 0 & 0\end{bmatrix} \tag{13}$$

where the impedance matrix Z is described as follows:

$$Z = \begin{bmatrix} Z_1 & jwk_{12}\sqrt{L_1L_2} & jwk_{13}\sqrt{L_1L_3} & jwk_{14}\sqrt{L_1L_4} \\ jwk_{12}\sqrt{L_1L_2} & Z_2 & jwk_{23}\sqrt{L_2L_3} & jwk_{24}\sqrt{L_2L_4} \\ jwk_{13}\sqrt{L_1L_3} & jwk_{23}\sqrt{L_2L_3} & Z_3 & jwk_{34}\sqrt{L_3L_4} \\ jwk_{14}\sqrt{L_1L_4} & jwk_{24}\sqrt{L_2L_4} & jwk_{34}\sqrt{L_3L_4} & Z_4 \end{bmatrix} \tag{14}$$

with

$$\begin{cases} Z_1 = R_S + R_1 + jwL_1 \\ Z_2 = R_{L2} + R_{C2} + j[wL_2 - 1/(wC_2)] \\ Z_3 = R_{L3} + R_{C3} + j[wL_3 - 1/(wC_3)] \\ Z_4 = R_{load} + R_4 + jwL_4 \\ w = 2\pi f \end{cases}.$$

The Q-factors of the transmitter and receiver can be obtained as follows, respectively:

$$Q_i = \frac{1}{R_{Li} + R_{Ci}}\sqrt{\frac{L_i}{C_i}} = \frac{Q_{Li}Q_{Ci}}{Q_{Li} + Q_{Ci}}\ (i = 2,\ 3) \tag{15}$$

with

$$Q_{Li} = \frac{wL_i}{R_{Li}},\ Q_{Ci} = \frac{1}{R_{Ci}wC_i}\ (i = 2,\ 3)$$

where Q_{Li} and Q_{Ci} ($i = 2,\ 3$) represent the respective Q-factors of coil L_i and capacitor C_i. By substituting equation (15) into equation (14), the impedance matrix at the resonant frequency $f = (2\pi L_iC_i)^{-1}$ ($i = 2, 3$) can be deduced

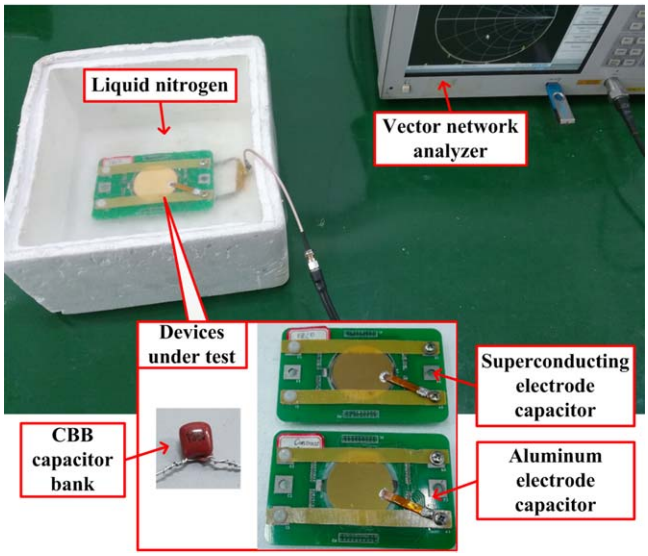

Figure 6. Overview of the HTS capacitor and contrasting capacitors. Liquid nitrogen is used to achieve a 77 K testing environment if necessary.

as:

$$Z = \begin{bmatrix} Z_1 & jwk_{12}\sqrt{L_1L_2} & jwk_{13}\sqrt{L_1L_3} & jwk_{14}\sqrt{L_1L_4} \\ jwk_{12}\sqrt{L_1L_2} & wL_2/Q_2 & jwk_{23}\sqrt{L_2L_3} & jwk_{24}\sqrt{L_2L_4} \\ jwk_{13}\sqrt{L_1L_3} & jwk_{23}\sqrt{L_2L_3} & wL_3/Q_3 & jwk_{34}\sqrt{L_3L_4} \\ jwk_{14}\sqrt{L_1L_4} & jwk_{24}\sqrt{L_2L_4} & jwk_{34}\sqrt{L_3L_4} & Z_4 \end{bmatrix}. \tag{16}$$

The currents of each loop circuit can be derived as:

$$\begin{bmatrix} \dot{I}_1 & \dot{I}_2 & \dot{I}_3 & \dot{I}_4 \end{bmatrix} = \begin{bmatrix} \dot{V}_S & 0 & 0 & 0 \end{bmatrix} \cdot Z^{-1}. \tag{17}$$

Thus, the efficiency of the WPT system is defined as follows:

$$\eta = \frac{P_o}{P_i} \times 100\% = \frac{|\dot{I}_4|^2 \cdot R_{Load} \times 100\%}{|\dot{V}_S \cdot \dot{I}_1| - |\dot{I}_1|^2 \cdot R_S}. \tag{18}$$

Also, η can be denoted by the S_{21}-parameter which can be measured directly by a vector network analyzer (VNA):

$$\eta = \frac{P_o}{P_i} \times 100\% = S_{21}^2 \times 100\%. \tag{19}$$

In order to verify the validity of the experimental results, we compared the measured data of the WPT efficiency based on equation (19) with the calculated value obtained from equation (18). To ensure the calculation accuracy, the parameters of the coils and capacitors were also measured by VNA. More details are provided in section 4.2.

4. Comparative experiments and discussions

4.1. Measured characteristics of the HTS capacitor

4.1.1. Experimental setup. To evaluate the characteristics of the proposed HTS capacitor, comparative experiments were carried out between the HTS capacitor and two contrasting capacitors, as shown in figure 6. Since the most common material of a capacitor electrode plate is aluminium (Al), one of the selected contrasting capacitors was an Al electrode capacitor ('Al capacitor' for short) based on doubled-sided Al thin film which was deposited on a $LaAlO_3$ substrate and also coated with Au surface layers. For the purpose of comparison, the structure, specifications and main components of the Al capacitor were designed as similar as possible to those of the HTS capacitor, except substituting YBCO layers with Al layers. A CBB capacitor bank was chosen as the other contrasting capacitor whose capacitance was close to that of the HTS capacitor, since the CBB capacitor is a commercial capacitor widely used at high frequency.

The impedance of the capacitor under test is measured by VNA. Then, the effective capacitance, ESR, and Q-factor can be obtained based on (3) and (7). While the comparison between the Al capacitor and HTS capacitor can reflect the effect of the HTS electrode material on the capacitor, that between the CBB bank and HTS capacitor can indicate the performance differences between these two capacitors.

4.1.2. Characteristic comparison. While the HTS capacitor and Al capacitor were both tested at different temperatures, including 77 K and a normal temperature (NT) of about 300 K, the CBB bank was tested only at its normal working temperature, NT. Figure 7(a) shows the measured capacitance of the capacitor in these cases versus frequency from 2–10 MHz. A capacitance decline of about 1.5% appears when the HTS capacitor or Al capacitor is submerged into liquid nitrogen from the normal environment. It is caused mainly by the relative permittivity decrease of the $LaAlO_3$ substrate with the environment temperature changing from NT to 77 K. Due to the unavoidable fabrication error of the substrate thickness, the capacitance of the Al capacitor is about 1.4% smaller than that of the HTS capacitor at the same temperature. The capacitance of the CBB bank is closer to that of the HTS capacitor at NT or the Al capacitor at 77 K.

The measured ESRs of the capacitors are indicated in figure 7(b). The HTS capacitor has the smallest ESR at 77 K with HTS electrode plates in the superconducting state, while it has a much bigger ESR at NT. The ESR of the Al capacitor is smaller at 77 K due to a decrease in the Al electric resistivity. Note that the ESR of the CBB bank becomes remarkably lower versus frequency, while those of the other capacitors change in an increasing trend. Considering that the conductive loss becomes higher with the increasing frequency, it can be explained that a major loss of the CBB capacitor is derived from the polypropylene dielectric layer whose loss tangent reaches 10^{-3} level at NT, and this dielectric loss would decrease at a higher frequency. In contrast, the losses of other capacitors are caused much more by the electrode plates than the dielectric layer ($LaAlO_3$) whose loss tangent is fairly small, nearly at 10^{-4} level at NT as well as 10^{-5} level at 77 K.

The Q-factor of the capacitor can be calculated based on equation (7) by dividing the imaginary part of the measured impedance to the real part, as presented in figure 7(c). It is found that the HTS capacitor at 77 K has the highest Q-factor

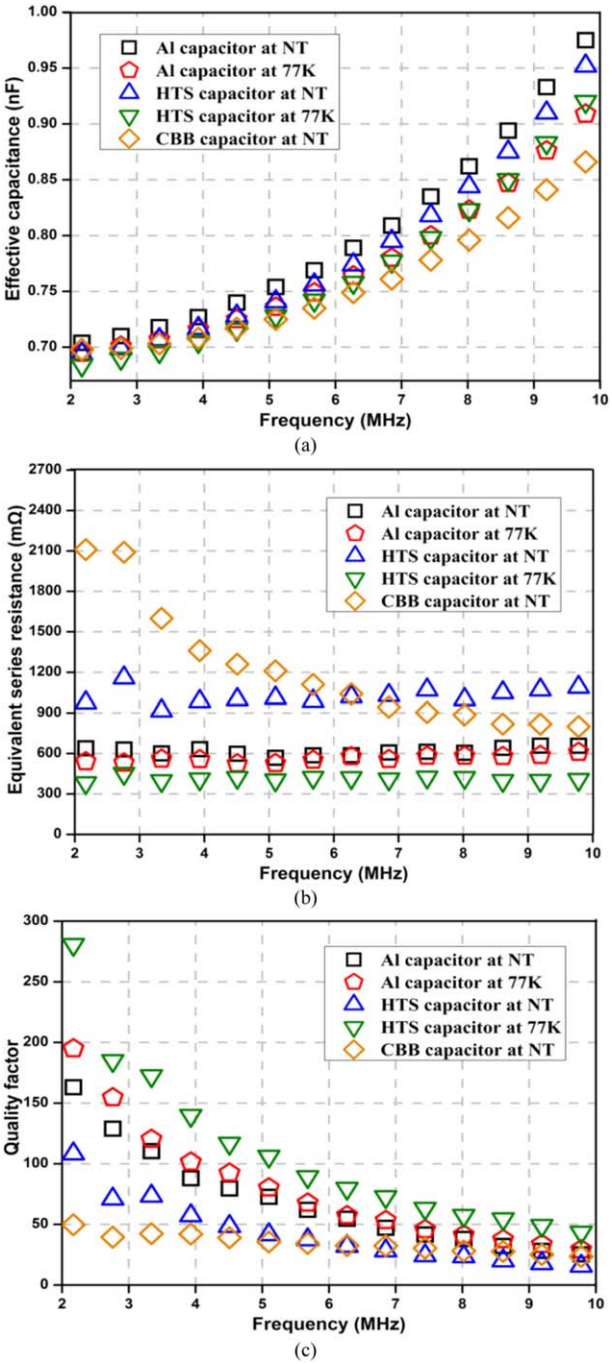

Figure 7. Measured characteristics of the HTS capacitor and contrasting capacitors. (a) Effective capacitance. (b) ESR. (c) Q-factor.

over the testing frequency range, about 96% ∼ 198% higher than that at NT, 13% ∼ 96% than the Al capacitor at NT, 11% ∼ 77% than the Al capacitor at 77 K, and 56% ∼ 499% than the CBB bank. These gaps attain the maximum at 2 MHz and minimum at 10 MHz, namely the high Q-factor property of the HTS capacitor would be more remarkable at a lower frequency.

In conclusion, the proposed HTS capacitor is found to have a higher Q-factor at 77 K, but a lower one at NT or at a higher frequency. Furthermore, due to the lower losses caused by the electrode plates and the dielectric layer, the HTS capacitor could have a higher Q-factor than the normal capacitor with equal volume.

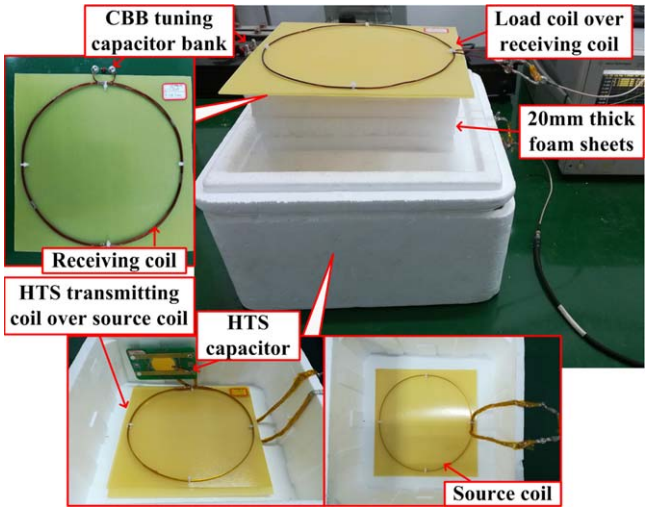

Figure 8. Experimental arrangement of the WPT test system with the HTS capacitor. While the source coil was under the transmitting coil, the load coil was placed over the receiving coil.

4.2. Effect of the HTS capacitor on the WPT system

4.2.1. Experimental arrangement. To investigate the effect of the proposed HTS capacitor, a test system based on figure 4 was constructed, as shown in figure 8. Comparative experiments were performed with the system operating successively in cases from 1–6, as shown in table 2, respectively. The component specifications of the WPT system are listed in table 3. Both the source coil and transmitting coil were made of HTS tape whose characteristic parameters are presented in table 4, while the receiving coil and load coil were made of 2 mm-thick cylindrical copper wire. The HTS tape was manufactured on the basis of encasing multi-filamentary bismuth-based HTS wire in a silver alloy matrix, and then covering with a protective layer of polyimide film for the sake of electrical insulation. All coils were fixed onto 0.5 mm-thick epoxy resin boards, respectively, and the distance between the source coil and transmitting coil, as well as that between the receiving coil and load coil, were both set at 0.5 mm, namely $d_{12} = d_{34} = 0.5$ mm.

According to equation (19), the transfer efficiency of the WPT system can be obtained from the S_{21}-parameter measured by VNA. To research the efficiency at the resonant frequency versus delivery distance d_{23}, three 20 mm-thick foam sheets were stacked in turn to lift both the receiver and load coil, changing d_{23} from 145 mm to 205 mm.

4.2.2. Tuning process. The operating frequency of the WPT system was designed at 2.5 MHz. However, it was hard for the WPT system in all cases to work at the same frequency due to the capacitance gaps of about 1.4% between the HTS capacitor and contrasting capacitors. In order to achieve the magnetic resonance, several CBB banks were respectively

Table 2. Different operating cases of the WPT test system.

Case no.	Capacitor of the transmitter	Environment of the capacitor	Environment of the transmitting coil and source coil	Transmitter resonant frequency (MHz)
1	Al	NT	NT	2.480
2	Al	77 K	77 K	2.500
3	HTS	NT	NT	2.505
4	HTS	77 K	77 K	2.540
5	CBB	NT	NT	2.505
6	CBB	NT	77 K	2.715

The terms Al, HTS, and CBB denote the Al electrode capacitor, HTS electrode capacitor, and CBB capacitor bank, respectively, and NT represents the normal temperature of about 300 K.

Table 3. Specifications of the WPT test system.

Component	Turns	Inductance (μH)	ESR (Ω)
Load coil at NT	1	0.91	0.14
Receiving coil at NT	3	5.72	0.38
Transmitting coil at NT	3	6.08	0.49
Transmitting coil at 77 K		6.08	0.30
Source coil at NT	1	1.04	0.19
Source coil at 77 K		1.05	0.12
Component	**Capacitance (nF)**	**ESR (Ω)**	**Q-factor**
HTS capacitor at NT	0.70	1.01	89
HTS capacitor at 77 K	0.69	0.46	197
Al capacitor at NT	0.71	0.57	157
Al capacitor at 77 K	0.70	0.55	163
CBB capacitor bank at NT	0.70	1.96	46
Optional tuning capacitor banks for the receiver at NT	0.68, 0.74, 0.76, 0.77	2.10, 1.51, 1.42, 1.37	45, 57, 59, 60

The radii of the coils are all 11.0 mm. All electrical parameters are measured at 2.5 MHz.

Table 4. Main parameters of the Bi2333/Ag tape used in the HTS coils.

Parameter	Value	Unit
Average width	4.3	mm
Average thickness	0.23	mm
Critical current (77 K, self-field)	185	A
Critical current density	1.87×10^{10}	A m^{-2}
Minimum double bend diameter	100	mm
Maximum rated tensile stress	65	MPa

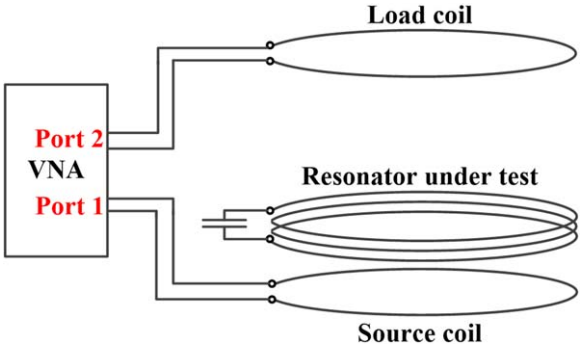

Figure 9. Test system for measuring the resonant frequency of the resonator.

used to tune the resonant frequency of the receiver as close as possible to that of the transmitter in different cases.

The resonant frequency of the transmitter in all these cases can be obtained by the test system in figure 9, and the measured values are also listed in table 2. Moreover, the resonant frequency of the tuned receiver can be observed with this system so that the magnetic resonance coupling between the receiver and transmitter can be achieved by adjusting the capacitance of the tuning capacitor bank for the transmitter resonant frequency. The WPT system in cases 2, 3, and 5 was tuned at a resonant frequency of nearly 2.5 MHz, with the receiver tuning capacitor blank of 0.76 nF capacitance and 47 Q-factor, while its resonant frequency in cases 1, 4, and 6 was tuned at 2.480, 2.54, and 2.715 MHz, with tuning capacitor blanks of 0.77, 0.74, and 0.68 nF capacitance as well as 59, 57, and 45 Q-factor, respectively.

4.2.3. Result analysis. With the distance d_{23} fixed at 145 mm, the measured data of transfer efficiency η in cases 1–6 versus frequency are presented in figure 10(a), and the corresponding calculated data based on equation (18) with the parameters in table 2 substituted are shown in figure 10(b). The measured curves of η in cases 1–5 have $1\% \sim 2\%$ higher resonant

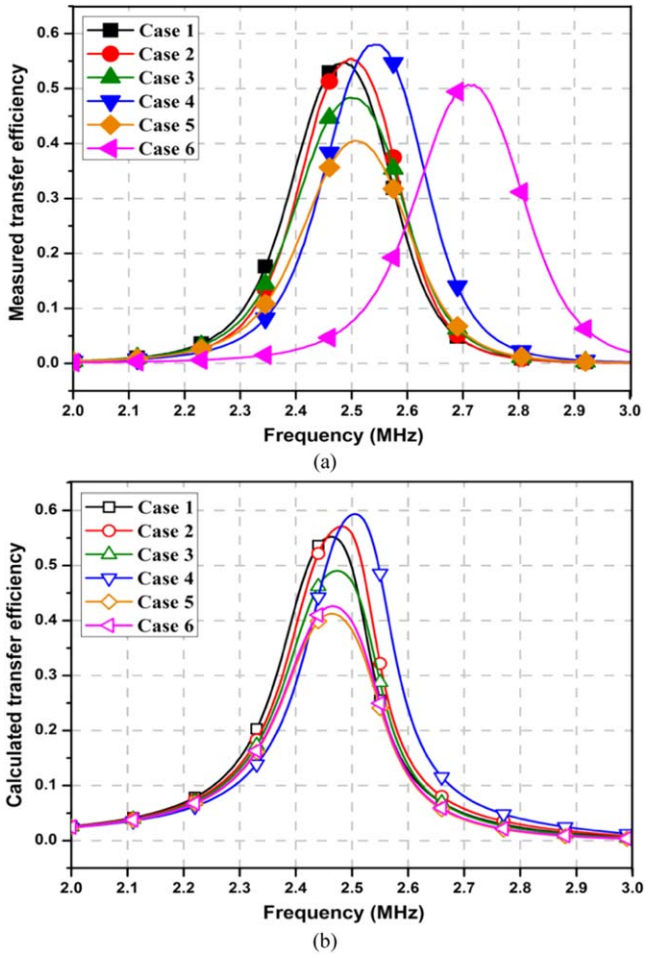

Figure 10. Comparison of the WPT efficiency η in cases 1–6 versus frequency with $d_{23} = 145$ mm. (a) Measured curves. (b) Calculated curves.

frequencies and $2\% \sim 3\%$ smaller peak values than the calculated ones, which is respectively due to the parasitic inductances and ohmic losses of the current lead joints between the resonant coil and capacitor. However, an abnormal difference exists in case 6 where the measured curve has an 8.4% higher resonant frequency and 18% larger peak value than the calculated one. This phenomenon implies a decrease in the capacitance and loss of the CBB bank. Namely, the CBB bank will be cooled by its current leads connected to the HTS coil at 77 K with its performance changing, even though it is placed in the external environment.

Figure 11 shows the system efficiency η_r at the resonant frequency versus d_{23} in all cases. The comparison results between the measured data and calculated ones are similar to that of figure 10, except that the difference caused by joints becomes larger as d_{23} increases. Note that the tuning capacitor bank of a smaller Q-factor will make the WPT efficiency lower. When such a capacitor bank is used, η_r in case 4 (with the HTS capacitor at 77 K) was measured under a more adverse condition, but still higher than that in case 2 (with the Al capacitor at 77 K), 4.6% at least with $d_{23} = 145$ mm and 8.4% at most with $d_{23} = 205$ mm. With other conditions

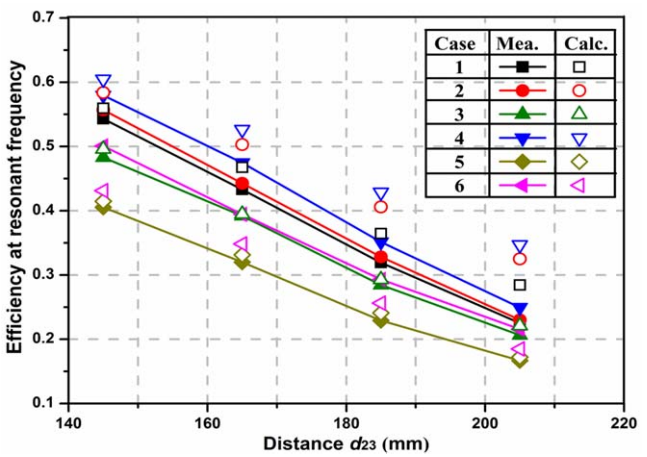

Figure 11. Comparison of the WPT efficiency η_r at resonant frequency in cases 1–6 versus d_{23}. The terms 'mea.' and 'calc.' denote the measured data and the calculated ones, respectively.

being equal, HTS electrode plates can even cause lower losses than the Al electrode plate at 77 K. In contrast to case 5, the HTS capacitor improves η_r $43\% \sim 50\%$ better than the CBB bank does. It is verified that the HTS capacitor can work with the HTS coil at 77 K, enhancing the η_r of the WPT system most remarkably among all comparative cases.

The η_r in case 3 is much smaller than that in case 4 owing to the larger resistance of the HTS material at NT. However, η_r in case 1 is just slightly smaller than that in case 2 due to the usage of a higher-Q tuning capacitor bank in case 1. Since the Q-factor of the CBB bank is much smaller than that of the HTS capacitor and the Al capacitor, even at NT, the WPT system has a much smaller η_r in case 5 than that in cases 1 and 3.

By comparing cases 5 and 6, the higher η_r in case 6 can be interpreted as the lower losses caused by the CBB bank cooled via its leads connected to the HTS coil at 77 K, as well as by the HTS coils at 77 K. The phenomenon whereby the resonant frequency in case 6 deviates 8.4% from that in case 5 is mainly due to the permittivity decline of the cooled CBB dielectric layer up to 15%. It might lead to a worse problem whereby such a capacitance deviation of the normal capacitor would cause the transmitter to decouple with the receiver at the design frequency and then the WPT system would work abnormally without a special tuning process (section 4.2.2).

In conclusion, it is experimentally confirmed that the HTS capacitor can improve the efficiency of the WPT system and work normally with the HTS coil at 77 K, and the relevant experiment results are consistent with the calculated data.

5. Conclusion

The proposed HTS capacitor based on double-sided YBCO thin film for WPT applications has been investigated in this paper. The Q-factor of the HTS capacitor at 77 K was measured $13\% \sim 96\%$ higher than that of the Al capacitor at NT over the frequency region from 2–10 MHz. Namely, the HTS capacitor has been found to provide a higher Q-factor than

capacitors made from normal material, and this property would be more remarkable at a lower frequency.

The effect of the HTS capacitor on the WPT system has been confirmed by comparative experiments. The HTS capacitor can enhance the WPT efficiency 4.6% ∼ 8.2% better than the Al capacitor does, and avoid the cooperation dilemma between the HTS coil and normal capacitor. Additionally, the all-superconducting resonator consisting of an HTS capacitor and HTS coil can be found to improve the WPT efficiency further by combining the low-loss advantages of these HTS devices. In summary, the proposed HTS capacitor has been proven to show potential for WPT applications.

Our future work will aim to develop a tunable HTS capacitor for WPT applications on the basis of the above findings and previous work regarding the SFS-based capacitor. For now, there is still a major obstacle for this type of capacitor (just as in [7, 8]) to work directly with the HTS coil, forming a tunable resonator, since the DC bias voltage across the ferroelectric substrate would bring a short-circuit fault to the HTS coil in connection. To achieve the tuning of the HTS capacitor based on an all-superconducting resonator for WPT technology, our focus will be on overcoming this short-circuit problem.

Acknowledgments

This work was supported by the Fundamental Research Funds for the Central Universities under grant 2682017ZDPY11.

ORCID iDs

Yingda He https://orcid.org/0000-0002-0963-4160
Yu Wang https://orcid.org/0000-0002-5391-8603
Yanwen Hu https://orcid.org/0000-0003-1557-6064
Zhongming Yan https://orcid.org/0000-0002-9879-2792

References

[1] Jin J X, Xin Y, Wang Q L, He Y S, Cai C B, Wang Y S and Wang Z M 2014 Enabling high-temperature superconducting technologies toward practical applications *IEEE Trans. Appl. Supercond.* **24** 5400712
[2] Coda N and Selvaggi J A 1976 Design considerations for high-frequency ceramic chip capacitors *IEEE Trans. Parts, Hybrids, Packag.* **12** 206–12
[3] Lindquist C S 1978 Capacitor DF and Q *IEEE Trans. Compon. Packag. Manuf. Technol.* **1** 115–7
[4] Mansour R R 2012 Microwave superconductivity *IEEE Trans. Microw. Theory Tech.* **50** 750–9
[5] Vendik I 2000 Phenomenological model of the microwave surface impedance of high-T_c superconducting films *Supercond. Sci. Technol.* **13** 974–82
[6] Jones W K, Olmedo R A, Hu Z Q and Larkins G Jr 1991 Development of superconducting electrode capacitor using a $YBa_2Cu_3O_{7-x}$ thick film and Y_2BaCuO_5 dielectric *IEEE Trans. Magn.* **27** 1619–21
[7] Karmanenko S F *et al* 1994 Formation and Raman spectroscopic study of YBCO/STO/YBCO heteroepitaxial structures *Supercond. Sci. Technol.* **7** 727–33
[8] Vendik O G, Hollmann E K, Zaitsev A G, Rauser D G and Petrov P K 1995 Preparation and properties of a capacitor structure formed by double-sided $YBa_2Cu_3O_{7-x}$ films on $SrTiO_3$ substrate *J. Phys. D: Appl. Phys.* **28** 1457–60
[9] Galt D, Price J C, Beall J A and Ono R H 1993 Characterization of a tunable thin film microwave $YBa_2Cu_{7-x}/SrTiO_3$ coplanar capacitor *Appl. Phys. Lett.* **22** 3078–80
[10] Karmanenko S F *et al* 1998 Patterning of tunable planar ferroelectric capacitors based on the YBCO/BSTO film structure *Supercond. Sci. Technol.* **11** 284–7
[11] Gao J, Zheng L, Fu X, Lin C and Yan R 1998 Ferroelectric characteristics of $Au/PbTiO_3/YBa_2Cu_3O_{7-\delta}$ and $Au/PbZr_{0.52}Ti_{0.48}O_3/YBa_2Cu_3O_{7-\delta}$ capacitors in a radiation environment *J. Phys. Condens. Matter* **10** 7493–9
[12] Xiao X Y, Liu Y, Jin J X, Li C S and Xu F W 2016 HTS applied to power system: benefits and potential analysis for energy conservation and emission reduction *IEEE Trans. Appl. Supercond.* **26** 5403309
[13] Schreiner F *et al* 2017 Design and manufacturing of a multistage cooled current lead for superconducting high current dc busbars in industrial *IEEE Trans. Appl. Supercond.* **27** 4802405
[14] Kurs A, Karalis A, Moffatt R, Joannopoulos J D, Fisher P and Soljačić M 2007 Wireless power transfer via strongly coupled magnetic resonances *Sci. Exp.* **317** 83–6
[15] Jeong I S, Jung B I, You D S and Choi H S 2016 Analysis of *S*-parameters in magnetic resonance WPT using superconducting coils *IEEE Trans. Appl. Supercond.* **26** 0501004
[16] Zhang G, Yu H, Jing L, Li J, Liu Q and Feng X 2014 Wireless power transfer using high temperature superconducting pancake coils *IEEE Trans. Appl. Supercond.* **24** 4600505
[17] Chung Y D, Lee C Y, Kang H K and Park Y G 2015 Design consideration and efficiency comparison of wireless power transfer with HTS and cooled copper antenna for electric vehicle *IEEE Trans. Appl. Supercond.* **25** 5000205
[18] Chung Y D, Lee C Y, Kim D W, Kang H K, Park Y G and Yoon Y S 2017 Conceptual design and operating characteristics of multi-resonance antennas in the wireless power charging system for superconducting maglev train *IEEE Trans. Appl. Supercond.* **27** 3601805
[19] Sedwick R J 2010 Long range inductive power transfer with superconducting oscillators *Ann. Phys.* **325** 287–99
[20] Lee K and Chae S H 2017 Effect of quality factor on determining the optimal position of a transmitter in wireless power transfer using a relay *IEEE Antennas Wireless Propag. Lett.* **27** 521–3
[21] Kim J, Son H C, Kim K H and Park Y J 2011 Efficiency analysis of magnetic resonance wireless power transfer with intermediate resonant coil *IEEE Antennas Wireless Propag. Lett.* **10** 389–92
[22] Hartwig W H 1973 Superconducting resonators and devices *Proc. IEEE* **61** 58–70
[23] Kedar A, Kataria N D and Gupta K K M 2004 Characterization and analysis of high temperature superconducting microstrip and coplanar resonators using a spectral domain method *Supercond. Sci. Technol.* **20** 408–12
[24] Khalil M S, Wellstood F C and Osborn K D 2011 Loss dependence on geometry and applied power in superconducting coplanar resonators *IEEE Trans. Appl. Supercond.* **21** 879–82
[25] Hua L, Lin F, Zhong H, Han Y and Kong Z 2009 Study on metallized film capacitor and its voltage maintaining performance *IEEE Trans. Magn.* **45** 327–30
[26] Jeong N S and Carobolante F 2017 Wireless charging of a metal-body device *IEEE Trans. Microw. Theory Techn.* **65** 1077–86
[27] Liu G, Mrad N, Xiao G, Li Z and Ban D 2012 Metallic environmental effect on RF-based energy transmission *IEEE Antennas Wireless Propag. Lett.* **11** 925–8